Applied Surface Science 254 (2008) 5501–5505

Contents lists available at ScienceDirect

Applied Surface Science

journal homepage: www.elsevier.com/locate/apsusc

Surface functionalization, morphology and thermal properties of polyamide6/O-MMT composite nanofibers by Fe_2O_3 sputter coating

Yibing Cai, Fenglin Huang, Qufu Wei *, Enci Wu, Weidong Gao

Key Laboratory of Eco-textiles, Ministry of Education, Jiangnan University, 1800 Lihu Avenue, Wuxi 214122, Jiangsu, People's Republic of China

ARTICLE INFO

Article history:
Received 24 January 2008
Received in revised form 26 February 2008
Accepted 26 February 2008
Available online 18 March 2008

Keywords:
Electrospinning
Sputter coating
PA6/O-MMT composite nanofibers
Surface morphology
Thermal stability

ABSTRACT

In the present work, the pure polyamide6 (PA6) nanofiber and PA6/organically modified montmorillonite (O-MMT) composite nanofiber were firstly prepared by a facile compounding process with electrospinning, and then coated by nanosize Fe_2O_3 using magnetron sputter technique. The effects of Fe_2O_3 sputter coating on structures, surface morphology and thermal stability were characterized by scanning electron microscope (SEM), X-ray photoelectron spectroscopy (XPS), energy dispersive X-ray spectroscopy (EDX), atomic force microscope (AFM) and thermogravimetric analyses (TGA), respectively. The SEM images showed that the diameters of composite nanofiber were decreased with the loadings of O-MMT and the nanosize Fe_2O_3 is well coated on the surface of the homogeneous and cylindrical nanofibers. The XPS spectra reflected the chemical features of the deposited nanostructures. The EDX confirmed the presence of the O-MMT and Fe_2O_3 in the fibers. The AFM observation revealed that there was a remarkable difference in the surface morphology of composite nanofiber before and after sputter coating. The TGA analysis indicated the barrier effects of silicate clay layers and catalysis effects of Fe_2O_3 improved thermal stability properties of the composite nanofiber.

1. Introduction

Nanofibers have interesting properties which are the result of their extremely high surface to weight ratio compared to the other conventional fibrous structures. These make nanofibers ideal for use in such application areas as filtration, sensor, protective clothing and functional materials, attributed to the high pore volume and tight pore sizes [1–7]. Polyamide 6 (PA6) is one of the most important engineering polymers manufactured in large quantities in various forms, such fibers, films, and plastics. PA6 accounts for a majority of the commercial polyamide production and application. The improvement of thermal and flammability properties of polymer nanofibers is a major concern in many practical applications. Among the most promising flame retardant additives are lammellar nanoparticles, particularly organoclays. The PA6 nanocomposites, loaded with only 1.6 wt% clay silicate layers, exhibited high strength, high modulus, high heat distortion temperature and low gas permeability compared to pure PA6 [8]. It is reported that the mechanical properties of the electrospun PA6/Na–montmorillonite fibrous mats were significantly improved, compared to the pure PA6 fibrous mats which was well studied using an atomic force microscope (AFM) [4].

Another emerging nanoparticles which have shown promising effects on polymer thermal degradation are metal oxides particles, such as Al_2O_3, TiO_2 and Fe_2O_3. The use of oxide particles in the submicronic or nanometric range as synergistic agents in addition to usual fire retardant additives seems to be very promising. It has been also noticed that their nanometric size made them suitable for synergistic effects with organoclays, allowing fire behavior performances to be improved [9–11].

In recent years, the sputtering technology has been widely used to deposit very thin films on various substrates for commercial and scientific purposes. The ability to deposit well-controlled coatings on nanofibers would expand the application of nanofibers, based on changes to both the physical and chemical properties of the nanofibers. In the present work, the electrospun PA6 composite nanofibers were modified with nanosize Fe_2O_3 by magnetron sputter coating. The effects of Fe_2O_3 sputter coating on structure and surface morphology were observed by scanning electron microscope (SEM), X-ray photoelectron spectroscopy (XPS) and AFM. The thermal properties of composite nanofibers were analyzed by thermogravimetric analyses (TGA).

2. Experimental

2.1. Materials

The organically modified montmorillonite (O-MMT) by hexadecyl trimethyl ammonium bromide (cation exchange capacity,

* Corresponding author. Tel.: +86 510 85912007; fax: +86 510 85913200.
E-mail address: qfwei@jiangnan.edu.cn (Q. Wei).

0169-4332/$ – see front matter © 2008 Elsevier B.V. All rights reserved.
doi:10.1016/j.apsusc.2008.02.185

CEC, 97 mequiv./100 g of clay) was purchased from Zhejiang Fenghong Clay Chemicals Co., Ltd. The average thickness of the particle was less than 25 nm, and the ratio of diameter to thickness was about 200. Polyamide6 (PA6, 1003NW8, with weight-average molecular weight 18,000, characteristic viscosity was 2.8) was supplied as pellets by UBE Industries, Japan. 99.5% *N*,*N*-dimethyl formamide (DMF) and 88% formic acid were all used as received.

2.2. Preparation of electrospun composite nanofibers

The slurry was prepared by dispersing O-MMT (2 g) powder into DMF (24.26 ml) solvent using magnetic stirring for 30 min until the powder uniformly dispersed in the DMF solvent, and then sonicated for 1.5 h. 15 wt% of PA6 dissolved in formic acid was also prepared. The prepared clay slurry was then put into the PA6 solution, which was mixed by magnetic stirring for 30 min and then was sonicated for another 20 min. The polymer solutions were electrospun at a positive voltage of 14 kV with a working distance of 10 cm (the distance between the needle tip and the collection plate), and an ejection rate of 0.2 ml/h. The mass ratio of the O-MMT to PA6 was 4 wt% and was referred to as PA6/O-MMT composite nanofiber.

2.3. Sputter coating

A magnetron sputter coating system JZCK-420B (Shenyang, Juzhi Co., Ltd.) was used to deposit a nanolayer on the composite nanofibers. A high purity Fe_2O_3 target (99.999%) was mounted on the cathode, and the nanofibers substrate was placed on the anode with a side facing the target. Argon pressure was set at 0.5 Pa. The radio frequency (RF) power used for Fe_2O_3 sputtering was set at 120 W. The thickness of the deposition layer was 100 nm, which was measured using Inficon XTM in situ film thickness monitor.

2.4. Characterization

SEM Quanta 200 was used to examine the structures of the composite nanofibers. The samples were coated with a thin layer of gold by sputtering before the SEM imaging. The SEM Quanta 200 equipped with energy dispersive X-ray spectroscopy (EDX) was used to examine the chemical compositions of the sputter coated nanofibers. An accelerating voltage of 20 kV with accounting time of 100 s was applied.

XPS were measured on a photoelectron spectrometer (ESCA Lab MK II instrument, UK) using Mg Kα radiation as the exciting source. The AFM was used to further observe the surface structures of the composite nanofibers. The AFM used in this work was a Benyuan CSPM 4000. Scanning was carried out in tapping mode. All images were obtained at ambient conditions.

TGA were carried out using a TGA50H thermo-analyzer instrument from 25 to 700 °C using a linear heating rate of 10 °C/min under nitrogen flow. The nitrogen flow was 25 ml/min. Samples were measured in a sealed alumina pan with a mass of about 10 mg.

3. Results and discussion

3.1. Structure and morphology

The SEM images of electrospun PA6 nanofiber and PA6/O-MMT composite nanofibers before sputter coating, collected on the aluminum foil, are illustrated in Fig. 1. The nanofibers are randomly distributed to form the three-dimensional fibrous web. It is observed that the electrospun nanofibers with variable fiber diameters. The morphology and average diameter of the electrospun PA6/O-MMT composite nanofibers are significantly affected by the amount of O-MMT added. Compared to the pure

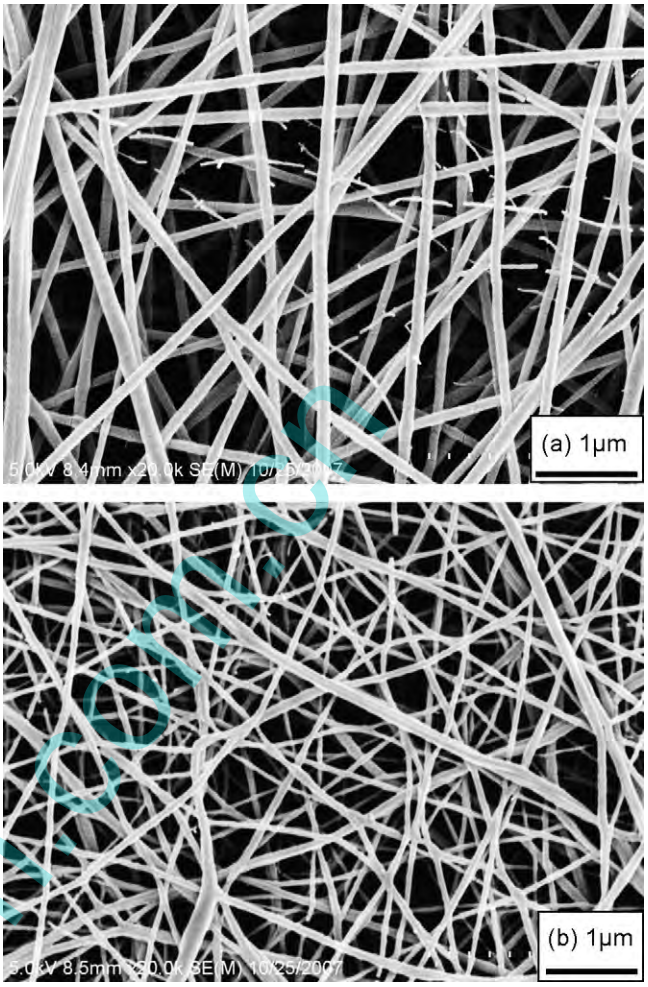

Fig. 1. SEM images of (a) pure PA6 nanofiber and (b) PA6/O-MMT composite nanofiber.

PA6 nanofibers, the average diameters of the PA6/O-MMT composite nanofibers are decreased with O-MMT loading.

The SEM images in Fig. 2 shows the structures of sputter coated nanofibers. It is observed that the ellipsoidal-like Fe_2O_3 nanoparticles are well deposited on the surface of nanofibers. Compared to the coated PA6 nanofibers with an average diameter of about 400 nm (Fig. 2a), the fiber diameters of the coated PA6/O-MMT composite nanofiber are reduced to about 300 nm, as indicated in Fig. 2b. This is because the addition of a quaternary ammonium salts as an organic modifier increases the charge density in ejected jets and thus stronger elongation forces are imposed to the jets because of the self-repulsion of the excess charges under the electrical field, resulting in substantially straighter shape and smaller diameter of electrospun fibers. Meanwhile, the conductivity of the PA6 solution is also another major factor affecting the morphology and diameter of the electrospun PA6 nanofibers. The loading O-MMT contained a quaternary ammonium ion ($C_{16}H_{33}(CH_3)_3N^+$) as an organic modifier and Na^+ and Ca^{2+} ions located between MMT layers, improves the conductivity of PA6/O-MMT solutions [12–14], leading to the decrease in the average diameter of the PA6/O-MMT composite nanofiber.

3.2. XPS analysis

XPS analysis reveals the compositions of the nanofiber surfaces. It is obvious that the main contents of the surface species are C, N, O and Fe as revealed in Fig. 3a. The main peaks are C 1s, N 1s and O 1s

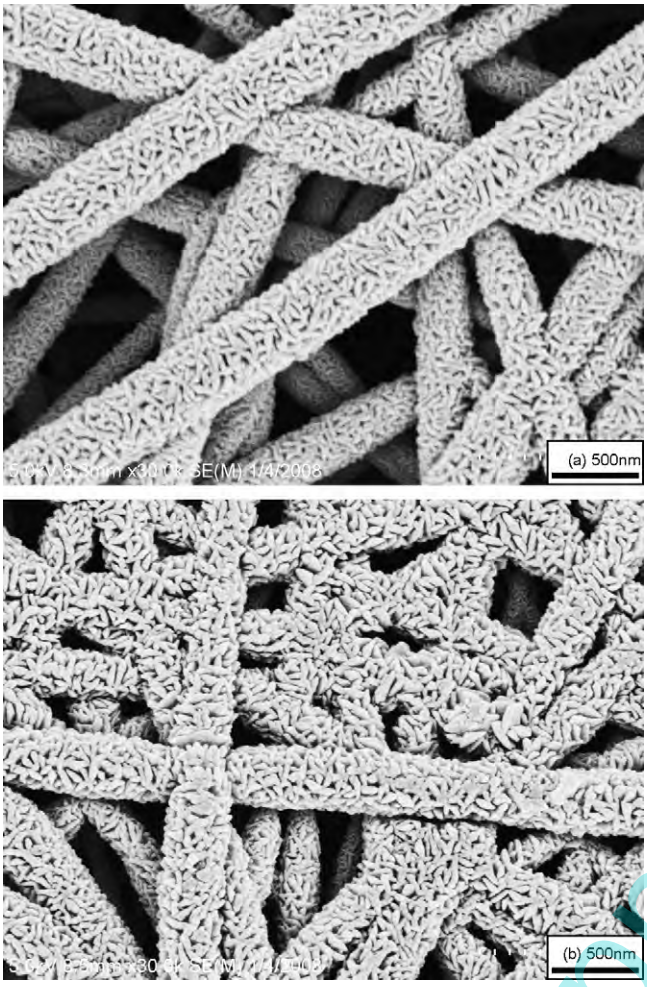

Fig. 2. SEM images of (a) coated PA6 nanofiber and (b) coated PA6/O-MMT composite nanofiber.

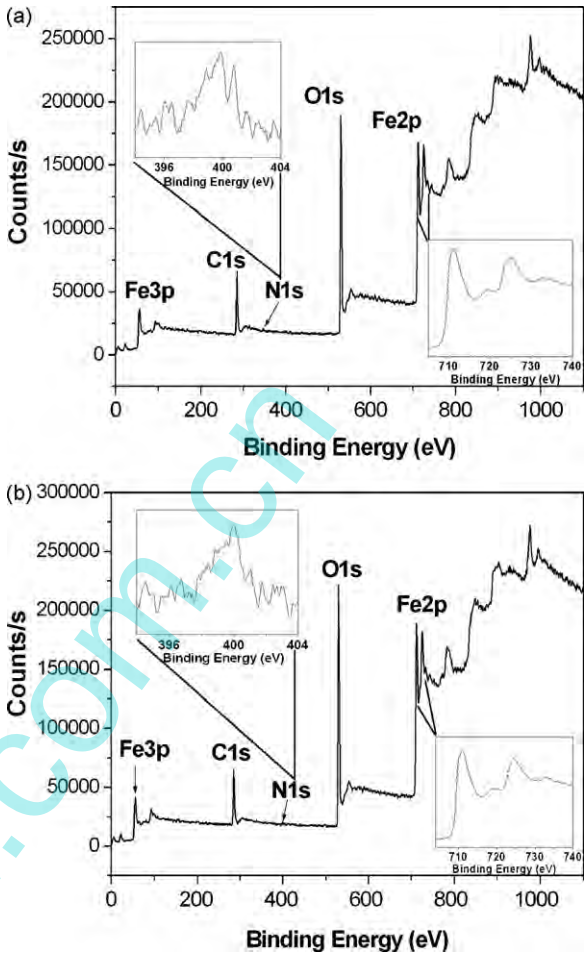

Fig. 3. XPS spectra of (a) coated PA6 nanofiber and (b) coated PA6/O-MMT composite nanofiber.

centered at 285, 400 and 530 eV, respectively. The XPS spectrum of Fe_2O_3-deposited nanofiber shows that two peaks are located at 710.9 and 724.9 eV, which are assigned to Fe 2p. The peak at about 52 eV corresponds to the Fe 3p. The binding energies of Fe 2p and Fe 3p peaks indicate that Fe_2O_3 is formed on the surfaces of the nanofibers. Meanwhile, the XPS spectrum of the coated PA6/O-MMT composite nanofibers is also shown in Fig. 3b. Comparing to XPS spectrum of the coated PA6 nanofibers (Fig. 3a), there are no obvious differences observed. Moreover, the binding energies at 104.1 eV for Si 2p (Si–O) and 73.8 eV for Al 2p (Al–O) of layer silicate clay [15] almost could not be detected. These results confirm that the silicate clay is not accumulated on the surface of composite nanofibers and is well dispersed within the composite nanofiber.

3.3. EDX analysis

The nanoclusters sputtered on the PA6 nanofiber surface are also confirmed by EDX analysis. Fig. 4 shows the EDX spectra of the coated PA6 nanofiber and coated PA6/O-MMT composite nanofiber. It can be seen that the coated fibers dominantly consist of C, O and Fe, deriving from the PA6 and the surface coated Fe_2O_3 nanoparticles, respectively. It can be also be observed that the amount of O becomes higher (Fig. 4b) compared with that in Fig. 4a, due to the contributions of O-MMT. Compared to the coated PA6 nanofiber, as illustrated in Fig. 4a, the significant amount of Al and Si within the PA6/O-MMT composite nanofiber can be seen in Fig. 4b. This is also attributed to the O-MMT within the nanofiber.

3.4. Surface morphology

The surface morphology of electrospun fibers before and after sputter coating is investigated using AFM. The AFM images of the uncoated PA6 nanofiber are presented in Fig. 5. The three-dimensional fibrous webs consist of many individual nanofibers with variable diameters and the fibers are randomly oriented in the web as illustrated in Fig. 5a. The AFM image reveals the relatively smooth surface with clear fibril structures of the fiber surface and formed a groove-like morphology. It is attributed to the effects of drawing and high shear flow during electrospinning. Sputter coating significantly alters the surface characteristics of the nanofibers, as indicated in Fig. 5b. It can be seen that the Fe_2O_3 nanoparticles are quite uniformly distributed on surface of the nanofiber. And the Fe_2O_3 nanoclusters with variable sizes form the rougher surface. The AFM image of the coated PA6/O-MMT composite nanofiber is shown in Fig. 5c. The Fe_2O_3 nanoparticles are also quite uniformly distributed on surface of nanofibers and the surface morphology also becomes rough after the sputter coating. The AFM image also reveals that the coated Fe_2O_3 nanoparticles the PA6/O-MMT composite nanofibers look more compact than those on the PA6 nanofibers. The loading of O-MMT reduces the interface tensions between the nanofibers and the nanosize Fe_2O_3, and is propitious to the depositions of Fe_2O_3

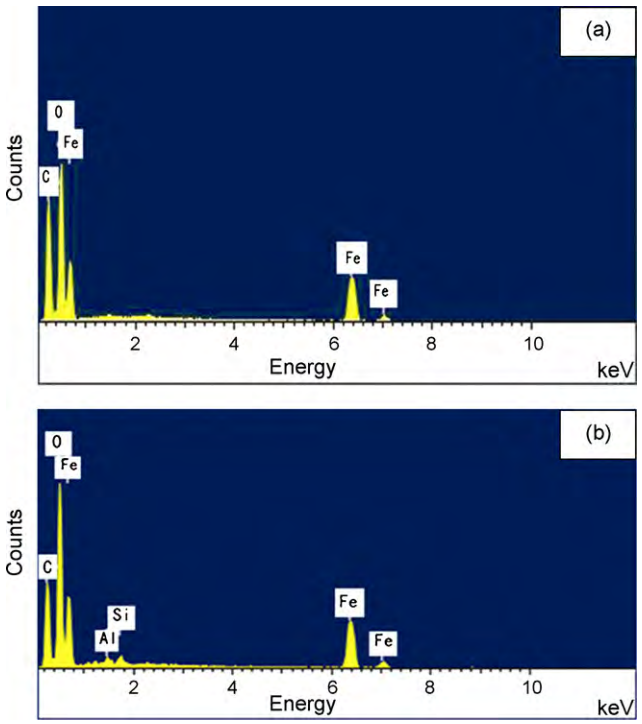

Fig. 4. EDX spectra of (a) coated PA6 nanofiber and (b) coated PA6/O-MMT composite nanofiber.

nanoparticles. The smoothness of the Fe_2O_3 film is improved and the sputtered film becomes more compact.

3.5. Thermal stability properties

Thermal stability of the electrospun fibers before and after sputter coating is evaluated using TGA in nitrogen atmosphere. The TGA curves for pure PA6 nanofiber, coated PA6 nanofiber and coated PA6/O-MMT composite nanofiber are shown in Fig. 6. It can be seen that the PA6 nanofibers before and after sputter coating display a one-step degradation. The onset degradation temperatures (defined as the temperature at 5 wt% weight loss) are, respectively, 402.2 °C (pure PA6 nanofiber), 354.9 °C (coated PA6 nanofiber) and 373.1 °C (coated PA6/O-MMT composite nanofiber). Compared to the pure PA6 nanofibers, the onset thermal stability of coated PA6 nanofiber and coated PA6/O-MMT composite nanofiber show a slight decrease. However, the thermal stability of coated PA6/O-MMT composite nanofiber is notably better than that of coated PA6 nanofiber. And the yield of charred residue at 700 °C for the coated PA6/O-MMT composite nanofibers is enhanced from 11.1% for the coated PA6 nanofiber to 16.3%. These results indicate that the cations of some transition metals (e.g., Fe^{3+}) may decrease the thermal stability of PA6 nanofiber and increase the charred residue. The effect is attributed to the ability of the cation to form complexes in which the metal atoms are coordinately bonded to the carbonyl oxygen atom of the amide group and are surrounded by polar solvent molecules [16]. The coated PA6/O-MMT composite nanofiber containing metal halides (the metal cations in the galleries of clay can couple with the Br^- in hexadecyl trimethyl ammonium bromide to form metal halides) starts to decompose at a lower temperature than pure PA6 nanofiber. However, it produced a substantially higher solid residue, which indicates extensive involvement of PA6 in the charring processes. These may be that the Fe^{3+} has catalysis effects on the degradation of PA6 [17]. It is also suggested that Fe^{3+} cations

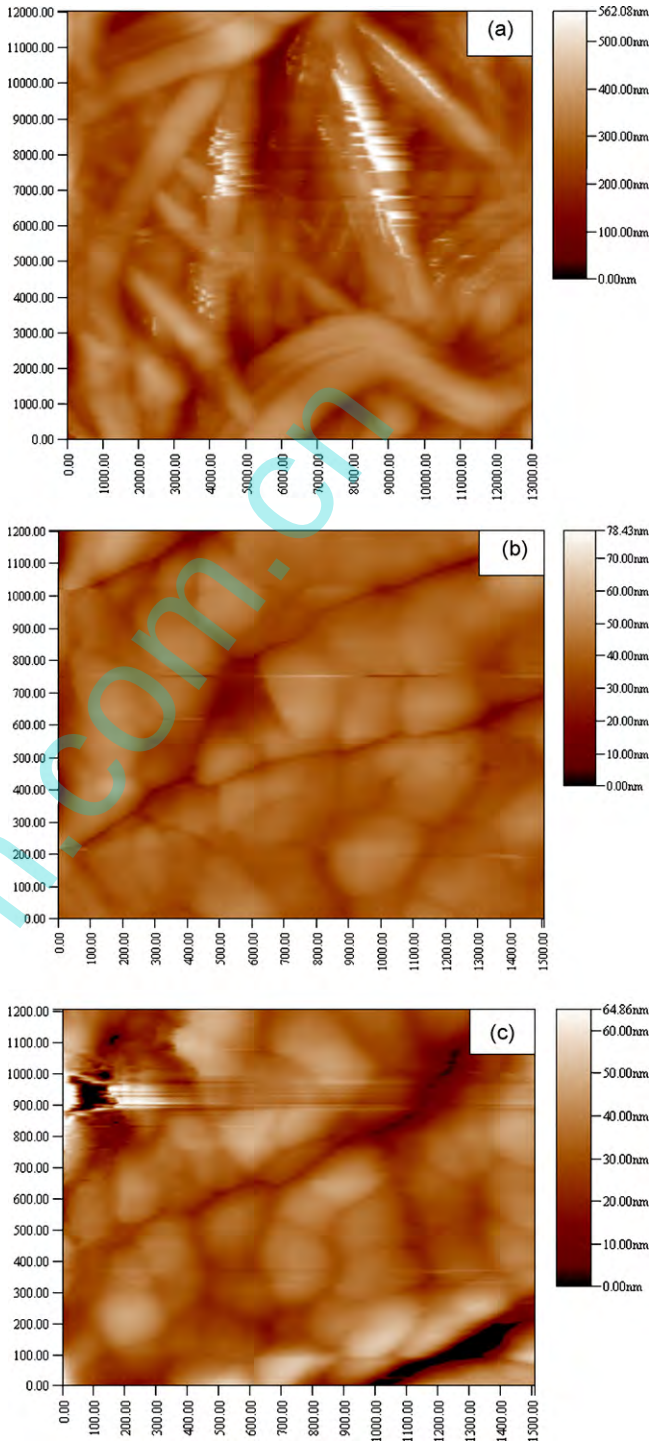

Fig. 5. AFM images of the (a) pure PA6 nanofiber, (b) coated PA6 nanofiber and (c) coated PA6/O-MMT composite nanofiber.

facilitate decomposition of hydroperoxides through a reversible oxidative–reductive catalytic process between Fe^{3+} and Fe^{2+} [18]. And, the Fe ion is also the operative site for radical trapping and increase thermal stability of coated PA6/O-MMT composite nanofibers [19]. Meanwhile, the increased charred residue contributes to the improved thermal stability of the coated PA6/O-MMT composite nanofibers. This is attributed to the nanosize silicate clay layers which could presumably facilitate the reassembly of lamellaes to form three-dimensional char, which might occur on the surface of the composite nanofibers and create

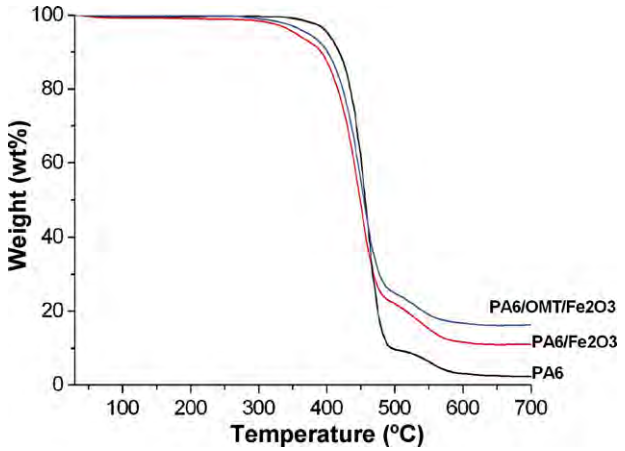

Fig. 6. TGA curves of the pure PA6 nanofiber, coated PA6 nanofiber and coated PA6/O-MMT composite nanofiber.

a physical protective barrier. Meanwhile, the silicate clay layers could act as a superior insulator and mass–transport barrier and subsequently mitigate the escape of volatile products generated during the thermal decomposition, contributing to the improved thermal stability properties of PA6 composite nanofibers [3,20].

4. Conclusions

The PA6/O-MMT composite nanofibers were prepared by a facile compounding and electrospinning. The surface functionalization of composite nanofibers was made by depositing well-controlled Fe_2O_3 nanoparticles using sputter coating. The influences of nanosize Fe_2O_3 on structural characteristics, surface morphology and thermal stability properties of the composite nanofibers were investigated. The diameters of composite nanofiber decreased with the loadings of O-MMT and the nanosize Fe_2O_3 well coated on the surface of homogeneous and cylindrical nanofibers. The XPS and EDX indicated the physical and chemical features of the deposited nanostructures. The AFM results indicated that there was a remarkable difference in the surface morphology of nanofibres before and after sputter coating. The TGA results revealed the improved thermal stability properties of the coated composite nanofiber, attributed to the superior insulator, mass–transport and physical protective barriers of silicate clay layers and catalysis effects of Fe_2O_3.

Acknowledgements

The work was financially supported by the Program for New Century Excellent Talents in University (No. NCET-06-0485), the specialized Research Fund for the Doctoral Program of higher education (No. 20060295005), Program for Innovative Team of Jiangnan University (PIRTJiangnan) and Program of Jiangnan University (No. 206000-21050737).

References

[1] H. Fong, W.D. Liu, C.S. Wang, R.A. Vaia, Polymer 43 (2002) 775.
[2] J.H. Hong, E.H. Jeong, H.S. Lee, D.H. Baik, S.W. Seo, J.H. Youk, J. Polym. Sci. Polym. Phys. 43 (2005) 3171.
[3] M. Wang, A.J. Hsieh, G.C. Rutledge, Polymer 46 (2005) 3407.
[4] L. Li, L.M. Bellan, H.G. Craighead, M.W. Frey, Polymer 47 (2006) 6208.
[5] G.M. Kim, G.H. Michler, F. Ania, F.J. Balta Calleja, Polymer 48 (2007) 4814.
[6] Y. Ji, B.Q. Li, S.R. Ge, J.C. Sokolov, M.H. Rafailovich, Langmuir 22 (2006) 1321.
[7] K.H. Yoon, M.B. Polk, B.G. Min, D.A. Schiraldi, Polym. Int. 53 (2004) 2072.
[8] N. Hasegawa, H. Okamoto, M. Kato, A. Norio Sata, Polymer 44 (2003) 2933.
[9] A. Laachachi, E. Leroy, M. Cochez, M. Ferriol, J.M. Lopez-Cuesta, Polym. Degrad. Stab. 89 (2005) 344.
[10] A. Laachachi, M. Cochez, M. Ferriol, J.M. Lopez-Cuesta, E. Leroy, Mater. Lett. 59 (2005) 36.
[11] A. Laachachi, M. Cochez, E. Leroy, P. Gaudon, M. Ferriol, J.M. Lopez-Cuesta, Polym. Adv. Technol. 17 (2006) 327.
[12] X.H. Zong, K. Kim, D.F. Fang, S.F. Ran, B.S. Hsiao, B. Chu, Polymer 43 (2002) 4403.
[13] W.K. Son, J.H. Youk, T.S. Lee, W.H. Park, Polymer 45 (2004) 2959.
[14] J.S. Choi, S.W. Lee, L. Jeong, S.H. Bae, B.C. Min, J.H. Youk, W.H. Park, Int. J. Biol. Macromol. 34 (2004) 249.
[15] I. Ravadits, A. Toth, G. Marosi, A. Marton, A. Szep, Polym. Degrad. Stab. 74 (2001) 419.
[16] P. Dunn, G.F. Sansom, J. Appl. Polym. Sci. 13 (1969) 1657.
[17] J. Liu, Y. Hu, S.F. Wang, L. Song, Z.Y. Chen, W.C. Fan, Colloid Polym. Sci. 282 (2004) 291.
[18] N.S. Allen, M.J. Harrison, M. Ledward, G.W. Fellows, Polym. Degrad. Stab. 23 (1989) 165.
[19] J. Zhu, C.A. Wilkie, Chem. Mater. 13 (2001) 4649.
[20] J.W. Gilman, C.L. Jackson, A.B. Morgan, R. Harris, E. Manias, E.P. Giannelis, Chem. Mater. 12 (2000) 1866.